Microscopic calculation of the multistep compound process

Toshihiko Kawano
Department of Advanced Energy Engineering Science, Kyushu University, 6-1, Kasuga-kouen, Kasuga 816-8580, Japan
(Received 8 September 1998)

The Feshbach, Kerman, and Koonin [Ann. Phys. (N.Y.) **125**, 429 (1980)] model of the statistical multistep compound (MSC) process is calculated microscopically, and comparisons of the microscopically calculated MSC process with a phenomenological phase-space model are made. The microscopic model gives a small particle emission probability in comparison with the constant wave function approximation, and a simple way to reconcile the difference is proposed. A $2p$-$1h$ doorway state formation cross section is calculated with the spherical Nilsson model, and a strength of the residual interaction V_0 is estimated from the doorway state formation cross section. The obtained V_0 is of the same magnitude as those derived in the previous multistep direct analyses. Comparisons of the microscopic MSC calculations with the experimental data show that the calculated particle emission spectra reproduce the measurements at backward angles. [S0556-2813(99)08602-1]

PACS number(s): 24.10.−i, 24.60.Dr, 24.60.Gv, 25.40.−h

I. INTRODUCTION

The quantum-mechanical theory of preequilibrium nuclear reaction by Feshbach, Kerman, and Koonin [1] (FKK) has a rather simple and feasible formulation in contrast with the theories of Tamura, Udagawa, and Lenske [2] and Nishioka, Weidenmüller, and Yoshida [3], and it has been applied to analyses of the medium- and high-energy nuclear reactions (see Ref. [4], for example). According to the FKK theory, particle emission is calculated from an incoherent sum of the multistep compound (MSC) process and the multistep direct (MSD) process. At low energies and large backward scattering angles, the MSD contribution had been regarded as negligible, and MSC analyses had been adopted to interpret double-differential cross section data [5,6]. Bonetti, Colli Milazzo, and Melanotte [7] applied the FKK theory to the double-differential cross-section data in the energy range of 13–18 MeV, and estimated the residual interaction strength V_0.

Chadwick and Young [8] showed in the analysis of ^{93}Nb data that the MSD component still persists at energies below 20 MeV, and the assumption that the MSC process dominates at backward angles can be invalid. The importance of the MSC emission is reduced, and only the first two steps of the MSC process, in addition to the MSD and the Hauser-Feshbach decay, were included [8] to analyze the experimental data.

In spite of the small contribution of MSC to the total emission spectra, an open question of physical interest still exists. A matrix element between the initial and final single-particle states contains a radial overlap integral. Originally, FKK assumed constant wave functions within a nucleus for a bound and an unbound particles, because it has a great advantage to evaluate the transition matrix element easily. More realistic wave functions were used in Ref. [9], and these authors developed a MSC code GAMME [10] which calculates the transition matrix elements microscopically. However, it has been pointed out that there is a considerable difference between the constant wave assumption and the realistic wave functions, and that a strength of the residual interaction, V_0, obtained from MSC analyses is quite different from the values used for MSD calculations.

The entrance strength function gives the probability of a doorway state excitation, which is proportional to V_0^2. Bonetti *et al.* [11] proposed a microscopic expression to evaluate the strength. Another expression was obtained by Chadwick and Young [8]. They introduced a factor R^{MSC} which is a fraction of flux into the initial bound $2p$-$1h$ state. The strength is calculated from an optical model transmission coefficient multiplied by R^{MSC}, and this expression does not depend upon V_0. These two expressions for the entrance strength should give a reasonable agreement, and from this agreement one can use the microscopic expression to estimate the V_0 values for the MSC process.

In Sec. II, we describe the formal MSC theory with two cases of treatment of the single-particle wave functions. Examples of the overlap integral calculation are shown in Sec. III to study the validity of the constant wave approximation, and the microscopic calculations of the entrance strength are provided to estimate the strength of residual interaction for the MSC process. Comparisons of the theoretical prediction with experimental data are shown in Sec. IV.

II. MICROSCOPIC DESCRIPTION OF THE MSC PROCESS

A. Particle emission spectrum

The MSC energy spectrum is given by [1]

$$\frac{d\sigma}{d\varepsilon}=\frac{\pi}{k^2}\sum_J (2J+1)2\pi\frac{\langle\Gamma_{1J}\rangle}{\langle D_{1J}\rangle} \times\sum_N \sum_{\nu j}\frac{\langle\Gamma_{NJ}^{\uparrow\nu j}\rho^{\nu}(U)\rangle}{\langle\Gamma_{NJ}\rangle}\prod_{M=1}^{N-1}\frac{\langle\Gamma_{MJ}^{\downarrow}\rangle}{\langle\Gamma_{MJ}\rangle}, \tag{1}$$

where N is the class of preequilibrium state, j is the angular momentum of the emitted particle, ν labels the three exit modes ($\Delta N=0$ and ± 1), $2\pi\langle\Gamma_{1J}\rangle/\langle D_{1J}\rangle$ is the entrance strength for producing bound $2p$-$1h$ states of spin J,

$\langle\Gamma^{\uparrow\nu j}_{NJ}\rho^{\nu}(U)\rangle$ is the escape width, $\langle\Gamma^{\downarrow}_{MJ}\rangle$ is the damping width, and $\langle\Gamma_{NJ}\rangle$ is the total width.

The escape and damping widths are factorized by X and Y functions, where the X function contains the possible angular momentum coupling and overlap integrals between the initial and final states. The Y function contains the possible phase space for the transition. The X and Y functions for the escape process $X^{\uparrow N\pm1}$, $X^{\uparrow N}$,$Y^{\uparrow N\pm1}$, and $Y^{\uparrow N}$, and for the damping process $X^{\downarrow N+1}$ and $Y^{\downarrow N+1}$, in which the number of excitons changes by $+2$ were defined by FKK in Ref. [1]. More practical and simple formulations are shown in Refs. [8] and [11]. The X functions for the escape process using the notations in Ref. [8] are

$$X^{\uparrow N+1j}_{NJ}=2\pi\frac{(2j+1)(2s+1)}{R_n(J)}\sum_{Qj_3j_4}(2j_3+1)(2Q+1)F(j_3)R_{n-1}(j_4)R_1(Q)\begin{pmatrix}j & Q & j_3\\ 0 & 0 & 0\end{pmatrix}^2\begin{Bmatrix}j & j_3 & Q\\ j_4 & J & s\end{Bmatrix}^2 I^2(Q,j_2,j_1,j), \tag{2}$$

$$X^{\uparrow Nj}_{NJ}=2\pi\frac{(2j+1)(2s+1)}{R_n(J)}\sum_{Qj_3j_4}(2j_3+1)(2Q+1)F(Q)R_{n-2}(j_4)R_1(j_3)\begin{pmatrix}j & j_3 & Q\\ 0 & 0 & 0\end{pmatrix}^2\begin{Bmatrix}j & j_3 & Q\\ j_4 & J & s\end{Bmatrix}^2 I^2(j_1,j_2,j_3,j), \tag{3}$$

$$X^{\uparrow N-1j}_{NJ}=2\pi\frac{R_{n-3}(s)}{R_n(J)}\sum_{Qj_3}(2j_3+1)(2Q+1)F(Q)R_1(j_3)\begin{pmatrix}j & j_3 & Q\\ 0 & 0 & 0\end{pmatrix}^2 I^2(j_1,j_2,j_3,j), \tag{4}$$

and for the damping process is

$$X^{\downarrow}_{NJ}=2\pi\sum_{jQj_3j_4}(2j+1)(2j_3+1)\frac{R_{n-1}(j_4)R_1(Q)R_1(j)}{R_n(J)}F(j_3)\begin{pmatrix}j & Q & j_3\\ 0 & 0 & 0\end{pmatrix}^2 I^2(Q,j_2,j_1,j)\Delta(Q,j_4,J), \tag{5}$$

where $F(Q)$ is the angular momentum density of a pair of states, $I(j_1,j_2,j_3,j)$ is the radial overlap integral, and $R_n(j)$ is the spin distribution given by

$$R_n(j)=\frac{2j+1}{2\sqrt{2\pi}\sigma_n^3}\exp\left\{-\frac{(j+1/2)^2}{2\sigma_n^2}\right\}, \tag{6}$$

with the spin cutoff parameter $\sigma_n^2=0.24nA^{2/3}$ [12].

B. Overlap integral

The radial overlap integral in Eqs. (2)–(5) with a zero-range interaction assumption is defined as

$$I(j_1,j_2,j_3,j)$$

$$=\frac{4}{3}\pi r_0^3V_0\frac{1}{4\pi}\int_0^{\infty}u_{j_1}(r)u_{j_2}(r)u_{j_3}(r)u_j(r)r^2dr, \tag{7}$$

where $u_{j_1}(r)$ and $u_{j_2}(r)$ are the radial parts of single-particle radial wave functions for the initial state, $u_{j_3}(r)$ and $u_j(r)$ are those for the final state, r_0 is the radius parameter taken to be 1.2 fm, and V_0 is the residual interaction strength.

According to the assumption made by FKK, the radial wave functions for the bound and unbound states are constant within the nuclear volume, so that

$$u_B(r)=\sqrt{\frac{3}{R^3}}\quad(r<R) \tag{8}$$

and

$$u_j(r)=\frac{4\pi}{(2\pi)^{3/2}}\frac{\sqrt{\mu kT_j}}{\hbar}, \tag{9}$$

where $R=r_0A^{1/3}$,μ is the reduced mass, k is the wave number of the emitted particle, and T_j is the transmission coefficient. The unbound wave function carries the single-particle state density of free particles [13] inside the nuclear volume $\mathcal{V}=4\pi R^3/3$; then

$$\int_0^R|u_j(r)|^2r^2dr=\frac{4\pi}{(2\pi)^3}\mathcal{V}\frac{\mu k}{\hbar^2}T_j\equiv\rho_c(E_c)T_j. \tag{10}$$

With the wave functions in Eqs. (8) and (9), one obtains analytical expressions of the radial overlap integrals in Eq. (7). The bound-unbound and bound-bound overlap integrals are [1]

$$I_j^2=\frac{1}{2\pi}\frac{4}{3}\frac{V_0^2r_0^3k\mu T_j}{\hbar^2A} \tag{11}$$

and

$$I_B^2=\frac{V_0^2}{A^2}. \tag{12}$$

To calculate the overlap integral with more realistic wave functions, the unbound wave function is replaced by a distorted wave [14] normalized in unit energy,

$$u_j(r)=\frac{4\pi}{(2\pi)^{3/2}}\frac{\sqrt{\mu k}}{\hbar}\frac{i}{2kr}\{H_j^*(r)-S_jH_j(r)\}\exp i\delta_l, \tag{13}$$

where $H_j(r)=G_j(r)+iF_j(r)$ is the outgoing-wave Coulomb function, S_j the scattering matrix element, and δ_l the Coulomb phase shift. In this paper, Eq. (13) is calculated with the Walter and Guss's global optical potential [15].

The bound wave function is calculated with a Woods-Saxon potential of $V=50$ MeV, $V_{so}=7$ MeV, $r=1.2$ fm, and $a=0.7$ fm. The quantum numbers and the binding energies of the bound states are determined according to the spherical Nilsson model with the parameters of Seeger and Howard [16].

Equation (10) implies that the unbound wave function is obtained by averaging of the l sum including the factor of $(2l+1)$ [17]. Thus the microscopic calculation of the overlap integral should be multiplied by $(2l+1)$ to allow a comparison of the two approaches.

A particle-hole configuration is selected according to energy, angular momentum, and parity conservation. There are several configurations for a possible transition for a given angular momentum transfer. The overlap integrals for all the possible transitions are averaged to give an appropriately averaged matrix element.

A more realistic interaction was introduced to calculate the overlap integral by Bonetti and Colombo [18]. The residual interaction of zero-range form in Eq. (7) was replaced by a Yukawa form, because it is possible to obtain an analytical expression of the matrix element [19]. The overlap integral becomes

$$I(j_1,j_2,j_3,j)=V_0\int_0^\infty\int_0^\infty u_{j_1}(r)u_{j_2}(r)g_L(r,r')u_{j_3}(r')u_j(r')r'^2dr'r^2dr, \tag{14}$$

where g_L is calculated from the modified Bessel functions,

$$g_L(r,r')=\begin{cases}(\mu r\mu r')^{-1/2}K_{L+\frac{1}{2}}(\mu r)I_{L+\frac{1}{2}}(\mu r') & (r\geqslant r')\\ (\mu r\mu r')^{-1/2}I_{L+\frac{1}{2}}(\mu r)K_{L+\frac{1}{2}}(\mu r') & (r<r'),\end{cases} \tag{15}$$

where μ^{-1} is the range of interaction.

C. Entrance strength function

In the MSC emission spectrum in Eq. (1), the emission probability and the damping probability can be calculated regardless to the residual interaction V_0, since V_0 cancels in the ratio of the emission and damping widths to the total width. The entrance strength still depends upon V_0, and one can evaluate the strength of V_0 if the entrance strength is calculated microscopically [11],

$$2\pi\frac{\langle\Gamma_{1J}\rangle}{\langle D_{1J}\rangle}=(2\pi)^2\omega(2,1,E)\sum_{Qj_3}(2Q+1)(2j_3+1)\times F(Q)R_1(j_3)\begin{pmatrix}j & j_3 & Q\\ 0 & 0 & 0\end{pmatrix}^2 I^2(j_1,j_2,j_3,j), \tag{16}$$

where $\omega(2,1,E)$ is the $2p$-$1h$ state density at the excitation energy E, and the angular momentum coupling scheme is defined in Fig. 1.

Chadwick and Young [8] proposed that the entrance strength can be evaluated by the optical model transmission coefficients corrected by a factor $R^{\mathrm{MSC}}=\omega^B(2,1,E)/\omega(2,1,E)$, which is the fraction of flux into the bound $2p$-$1h$ state. The entrance strength becomes

$$2\pi\frac{\langle\Gamma_{1J}\rangle}{\langle D_{1J}\rangle}=R^{\mathrm{MSC}}T_J. \tag{17}$$

III. RESULTS OF NUMERICAL CALCULATIONS AND DISCUSSIONS

A. Microscopic calculation of the overlap integral

The overlap integral for the entrance strength function in Eq. (16) describes a transition in which an incident particle of total spin j is captured in the shell model orbit j_1, creating a particle-hole pair j_2 and j_3, as shown schematically in Fig. 1. The energy of the final $2p$-$1h$ state is an excitation energy of the composite system given by $E_\mu=E_1+E_2-E_3$, where $E_i(i=1,2,3)$ is the binding energy of the particle or hole state. This configuration is only excited if the incident energy E_j is about the same as E_μ. We assume that the energy of $2p$-$1h$ state has a Gaussian distribution [4]

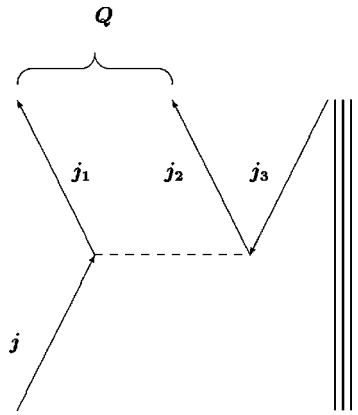

FIG. 1. The angular momentum coupling scheme for the entrance channel. The incident particle j is captured in the single-particle orbit j_1, creating the particle-hole pair j_2 and j_3.

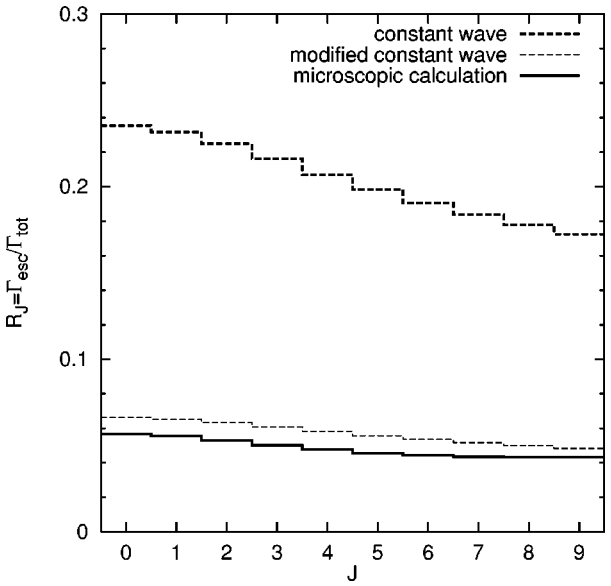

FIG. 2. Comparison of the ratio of the escape width to the total width for 14-MeV neutron-induced reactions on ^{93}Nb. The thick dashed line represents the calculated ratio with the constant wave approximation, the thick solid line is the microscopic calculation, and the thin dashed line is the result of the constant wave approximation in Eq. (22).

$$G(E_x,E_\mu)=\frac{1}{\sqrt{2\pi}\Gamma}\exp\left\{-\frac{(E_x-E_\mu)^2}{2\Gamma^2}\right\}, \tag{18}$$

with the spreading width Γ taken to be 4 MeV. This distribution is used for weighing to average the overlap integrals for all possible transitions.

A comparison of the escape widths calculated with the constant wave approximation and the microscopic model is shown in Fig. 2, which is the ^{93}Nb(n,n') reaction ($E_n=14$ MeV) at the first stage ($N=1$). The ratio of the escape width to the total width is expressed by

$$R_J=\sum_\nu \sum_j \int \frac{\langle \Gamma^{\uparrow\nu j}_{NJ}\rho^\nu(U)\rangle}{\langle \Gamma_{NJ}\rangle}dU. \tag{19}$$

The dependences of R_J on the total spin J for both the constant wave calculation and the microscopic calculation are similar, but they differ in the magnitude. The values for the microscopic calculation are about $\frac{1}{4}$ of those for the constant wave approximation.

In order to estimate an averaged squared matrix element with the constant wave approximation, which yields better results than Eq. (9), we recall the results obtained by Lee and Griffin [17]. The distorted wave normalized in unit energy is given by Eq. (13). Supposing the wave function inside the nucleus is constant, its amplitude is just the same value at the nuclear surface $r=R$. What we need is the average value of $|u_j(R)|^2$ over the phase shift taken from 0 to 2π. It is given by

$$\overline{|u_j(R)|^2}\simeq\frac{2}{\pi}\frac{\mu}{\hbar^2 k}\frac{1}{2}. \tag{20}$$

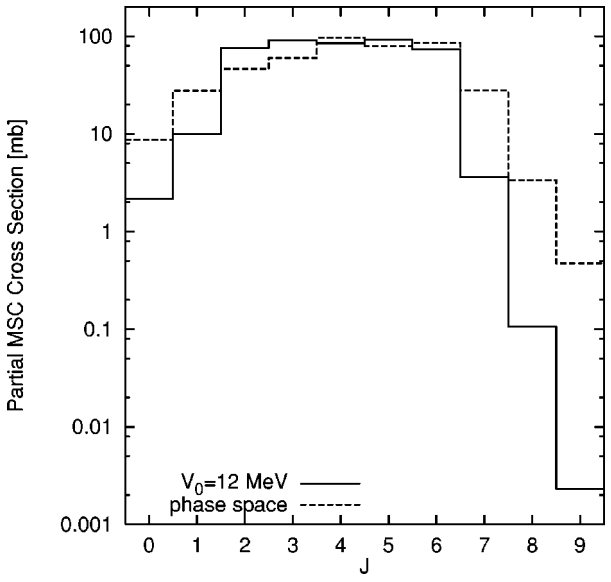

FIG. 3. Comparison of the partial MSC cross sections of 14-MeV neutron-induced reactions on ^{93}Nb. The solid line is the result of the microscopic calculation in Eq. (16), and the dashed line is the phase-space model in Eq. (17).

We can evaluate the smooth average of l sum of Eq. (20) with the approximation of $l_{max}\simeq kR$. For $kR\gg 1$, we have [20]

$$\sum (2l+1)\overline{|u_j(R)|^2}\simeq\frac{2}{\pi}\frac{\mu k}{\hbar^2}\frac{R^2}{2}=\frac{3}{R}\frac{1}{2}\rho_c(E_c). \tag{21}$$

Therefore the constant unbound wave becomes

$$u_j(r)=\frac{4\pi}{(2\pi)^{3/2}}\frac{\sqrt{\mu k T_j}}{\hbar}\sqrt{\frac{3}{R}\frac{1}{2}}. \tag{22}$$

The calculated R_J with Eq. (22) is shown in Fig. 2 by the light dashed line, which is in good accordance with the microscopic calculation.

B. Entrance strength function

The constant wave approximation has an advantage for calculations of a composite system decay rate because the computational time-requirement is much less than the microscopic calculation. However we cannot apply this approximation for calculations of the entrance strength, because the strength is not calculated from the ratio of the escape width to the total width, but it is proportional to the width of the $2p$-$1h$ doorway state.

Figure 3 shows the calculated strength for 14-MeV neutron-induced ^{93}Nb reaction (multiplied by $(2J+1)\pi/k^2$ to give an initial $2p$-$1h$ state formation cross section). The distorted wave and the transmission coefficient are calculated with the Walter-Guss global optical potential [15]. The single-particle state density parameter g is taken as $g=A/13$ MeV^{-1}, and the pairing energy correction $\Delta=0$. The solid line was calculated microscopically according to the coupling scheme in Fig. 1, and the dashed line was obtained from Eq. (17). The total reaction cross section of the microscopic calculation is normalized to the same value

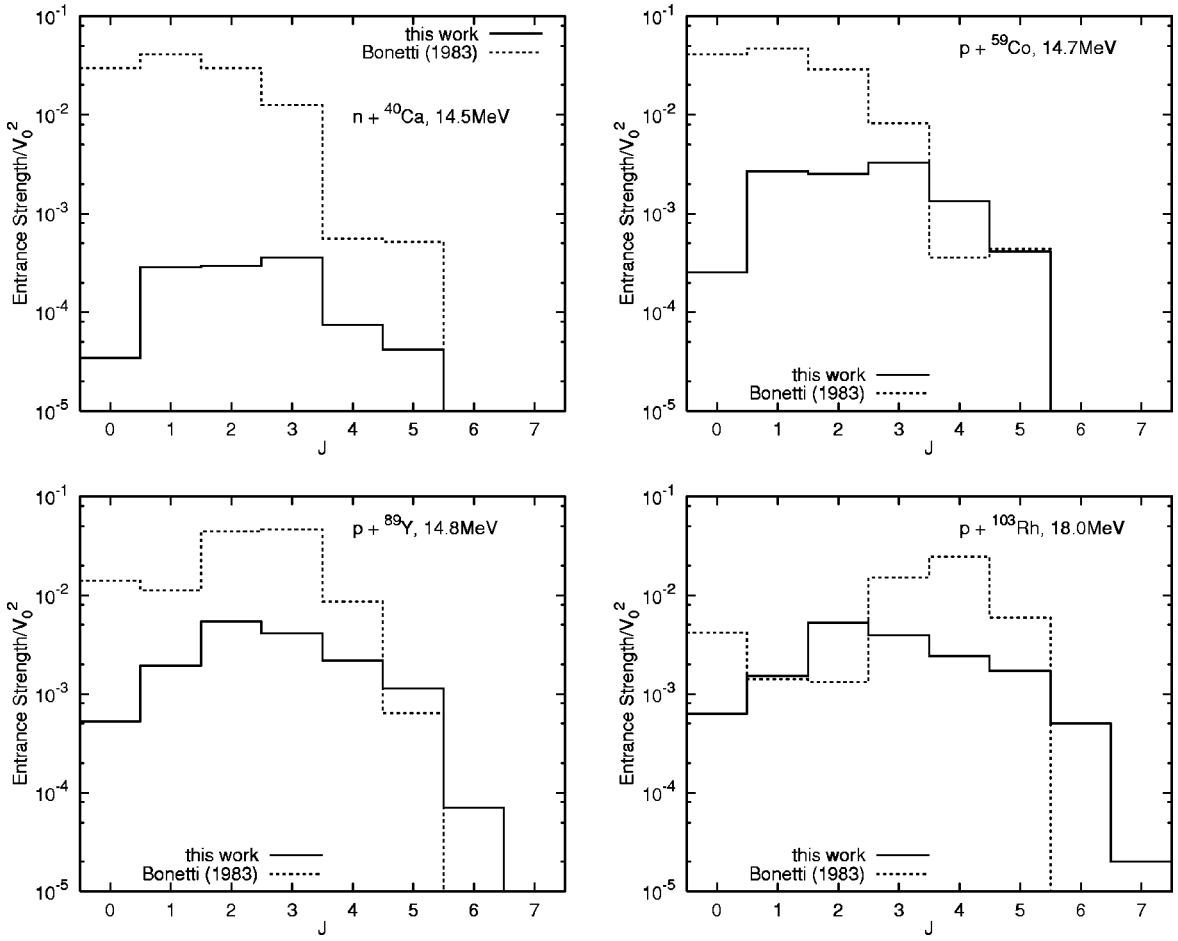

FIG. 4. Comparison of the entrance strength functions of 14.5-MeV neutron-induced ^{40}Ca, 14.7-MeV proton-induced ^{59}Co, 14.8-MeV proton-induced ^{89}Y, and 18.0-MeV proton-induced ^{103}Rh reactions, with those obtained by Bonetti, Colli Milazzo, and Melanotte (Ref. [7]).

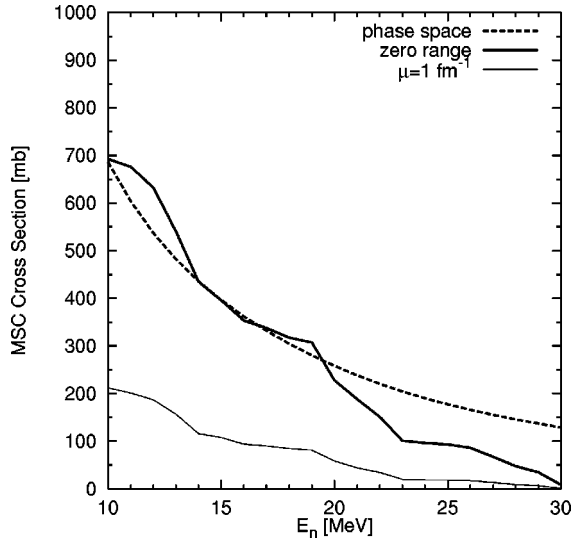

FIG. 5. Comparison of the $2p$-$1h$ doorway state formation cross sections of neutron-induced reactions on ^{93}Nb. The solid lines are the results of the microscopic calculation in Eq. (16) with $V_0 = 12$ MeV, and the dashed line is calculated with Eq. (17). The thick solid line represents the zero-range interaction, and the thin solid line is the Yukawa interaction with the range of 1 fm.

given by Eq. (17), and one obtains the value of $V_0 = 12.0$ MeV when the zero-range interaction in Eq. (7) is assumed. In the microscopic calculation, the particle and hole states which obey angular momentum and energy conservation are included. This restricts the possible final states, and results in small cross sections for large J.

There is a pioneering work of microscopic calculations of the entrance strength by Bonetti, Colli Milazzo, and Melanotte [7]. Comparisons of the calculated entrance strength functions for the ^{40}Ca$+n$, ^{59}Co$+p$, ^{89}Y$+p$, and ^{103}Rh$+p$ reactions are shown in Fig. 4, where the entrance strength is divided by V_0^2. One can see the large difference between the present results and those obtained in Ref. [7]. The difference is obvious for ^{40}Ca and ^{59}Co at small spins, and it tends to decrease as the target mass number increases. Both calculations are based on the shell model, however, Bonetti, Colli Milazzo, and Melanotte included a large number of orbits which are not expected from strict adoption of the shell model. This assumption allows a number of transitions of various angular momentum transfer, and it results in a large probability of the $2p$-$1h$ doorway state formation. On the other hand, our approach follows the shell model which restricts the possible transitions; then the doorway state formation probability becomes smaller, especially for the composite states with small spin. The obtained spin distributions become very similar to those given by the phase-space model, as seen in Fig. 3.

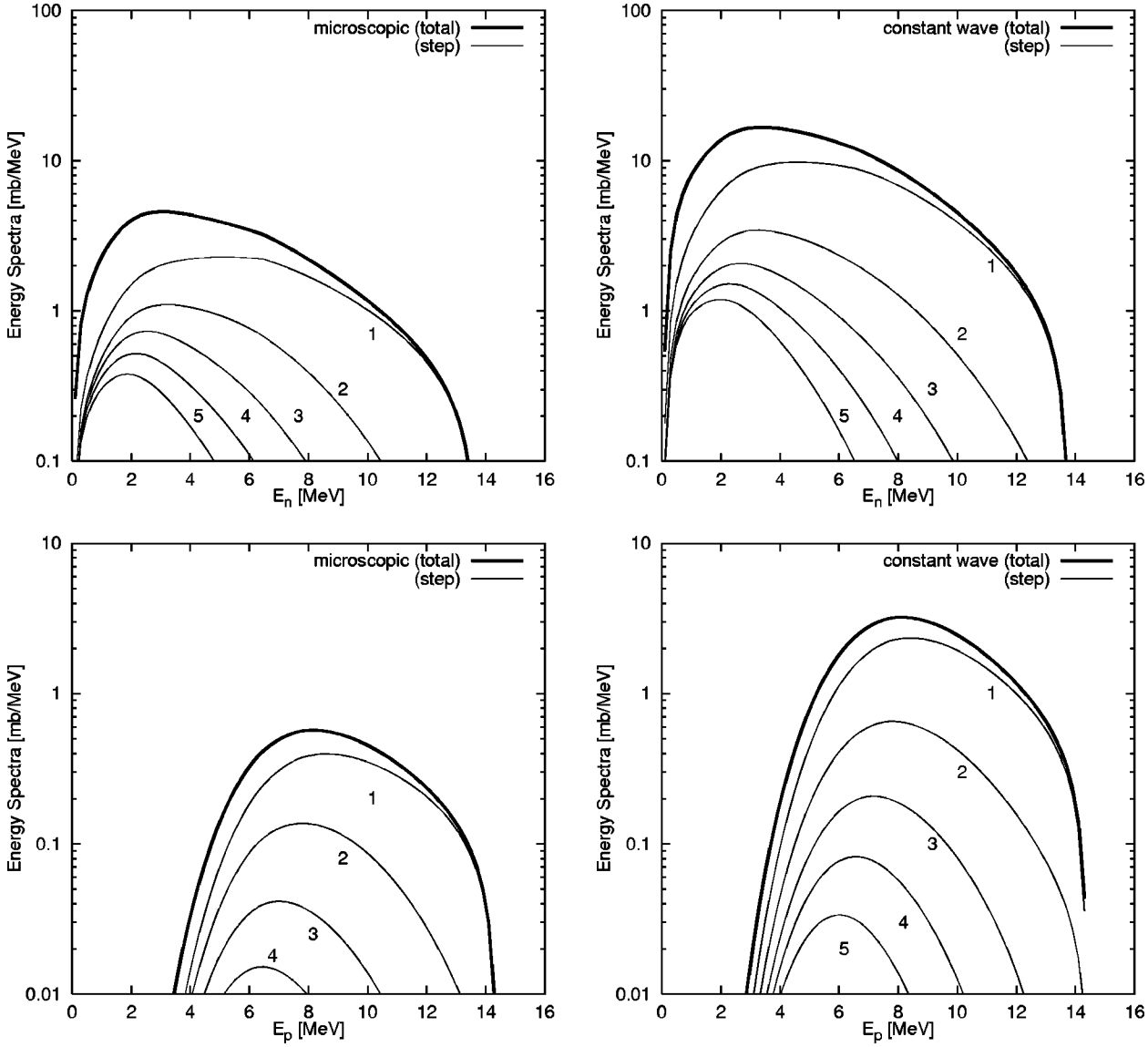

FIG. 6. Comparisons of the MSC emission spectra of neutron-induced reactions on ^{93}Nb up to five steps. The drawings on the left side are the results of the microscopic calculation, and those on the right side are calculated with the constant wave approximation.

C. Strength of the residual interaction

The $2p$-$1h$ doorway state formation cross section is proportional to V_0^2 when Eq. (16) is employed, and it is possible to estimate V_0 roughly if one compares the cross sections given by Eq. (16) and those given by Eq. (17). Figure 5 shows the $2p$-$1h$ state formation cross sections for neutron-induced ^{93}Nb reactions as functions of the incident energy. The thick solid line is calculated from Eq. (16) with $V_0 = 12.0$ MeV, and the dashed line is Eq. (17). The value of V_0 was chosen to give the same cross section at 14 MeV.

As shown in Fig. 5, the value of $V_0 = 12.0$ MeV gives the $2p$-$1h$ state formation cross sections those are reasonably in agreement with the phase space calculation of Eq. (17). This V_0 value is larger than the value of 5 MeV obtained by Bonetti, Colli Milazzo, and Melanotte [7] in their MSC analysis, but it is still smaller than values used in the recent MSD analyses [4,8,21]. Bonetti and Colombo [18] showed that the V_0 value increases when a Yukawa interaction with the range of 1 fm is adopted to calculate the matrix element. This is shown in Fig. 5 by the thin solid line. The effect of inclusion of the finite-range correction is very large, but it can be compensated for if one adjusts V_0 appropriately. The value of $V_0 = 23.3$ MeV yields approximately the same cross section as the zero-range calculation with $V_0 = 12.0$ MeV, and this value agrees $V_0 = 23.9$ MeV derived by Koning and Chadwick [4] from the FKK analysis of ^{90}Zr(n,xn) reaction data at 14 MeV.

Watanabe *et al.* [21] discussed an effect of the nonlocality correction [22] to the MSD cross sections, and they found that the correction reduces the MSD emission considerably. When the nonlocality correction is incorporated into the entrance strength calculation, it results in smaller $2p$-$1h$ state formation cross sections. The correction with the nonlocality $\beta = 0.85$ [19] reduces the cross sections to 40–60 %. This reduction can be compensated for by the larger V_0. The V_0 value of 30.0 MeV gives roughly the same cross section as the result without the nonlocality correction; however, this value is still smaller than the published values (39.3 MeV in Ref. [8] and 42.8 MeV in Ref. [21], for example) in which the nonlocality correction was incorporated.

D. Particle emission spectra

As demonstrated by Fig. 3, the phase-space model in Eq. (17) is a good approximation of the microscopic calculation of the entrance strength. We adopt Eq. (17) here to calculate the initial $2p$-$1h$ state formation cross section, then we can compare energy spectra of emitted particles regardless of the value of V_0 for both the microscopic calculation and the traditional constant wave-function approximation.

Figure 6 shows comparisons of the MSC particle emission spectra for 14-MeV neutron induced reactions on ^{93}Nb up to five steps. Parameters adopted for those calculations were Walter and Guss's global optical potential [15], the single-particle state density parameter $g=A/13$, and no pairing energy. The shape of the energy spectra, not only the total MSC emission spectra but also the emissions from various stages, is almost the same for both cases, and the difference mainly appears in the absolute values of the cross section. The microscopic calculation gives a smaller MSC emission probability than the constant wave approximation. This difference will be masked by the larger MSD emission and the Hauser-Feshbach statistical decay components in practical applications of the FKK theory to the experimental data.

The doorway state formation cross section in Fig. 6 is 436 mb, which is given by Eq. (17), and its 8% is emitted during the MSC process up to five steps when the process is calculated microscopically. In the case of the constant wave approximation, this fraction increases to 32%. As discussed in Sec. III A, if one introduces the factor of $3/2R$ into the constant wave calculations, this fraction decreases to 9%, which agrees with the microscopically calculated result. The calculated spectra with the constant wave approximation multiplied by $3/2R$ are shown in Fig. 7 by the thin dotted lines. The neutron emission spectra with the modified constant wave approximation is consistent with the microscopic calculation. The proton emission is still slightly larger, but the discrepancy between them becomes smaller.

The microscopic calculations with the Yukawa interaction of 1-fm range are shown in Fig. 7 by the thin solid lines. It was found that the differences between the zero-range and finite-range calculations are small for this case, although it has great influence on the entrance strength calculations, as shown in Fig. 5. The dot-dashed lines in Fig. 7 are calculated with the nonlocality correction as well as the finite-range interaction. The adopted nonlocality parameter is 0.85 [19]. The effect of this correction for emission process is also small.

Finally, we can conclude that the constant wave approximation for the MSC process gives almost the same cross sections as the microscopic calculation, if it is corrected by the factor of $3/2R$. The approximation has a great advantage for computation, because it reduces the radial overlap integrals which contain bound and unbound wave functions into the simple analytical expressions in Eqs. (8) and (9). Consequently, the computational time-requirement becomes very small. For example, almost 4 h were needed to calculate the MSC spectra with the Yukawa interaction in Fig. 7 with a modern workstation, while the constant wave calculation took only 5 s.

IV. COMPARISON WITH EXPERIMENTAL DATA

Comparisons of the microscopic MSC calculations with the experimental data are made for 14.1- and 18.0-MeV neutron-induced ^{93}Nb reactions [23]. At these energies the MSD emission competes with the MSC, but only the one-step component is important. The one-step MSD cross section is given by a weighted sum over squared DWBA matrix elements which excite a $1p$-$1h$ state. We adopt a traditional one-component theory to evaluate the one-step MSD emission. The DWBA matrix elements for various transitions are averaged to give an appropriate one-component matrix element, and the one-component state density formula of Williams [24] is employed. This approach is a simplified technique rather than the microscopic two-component theory of Koning and Chadwick [4].

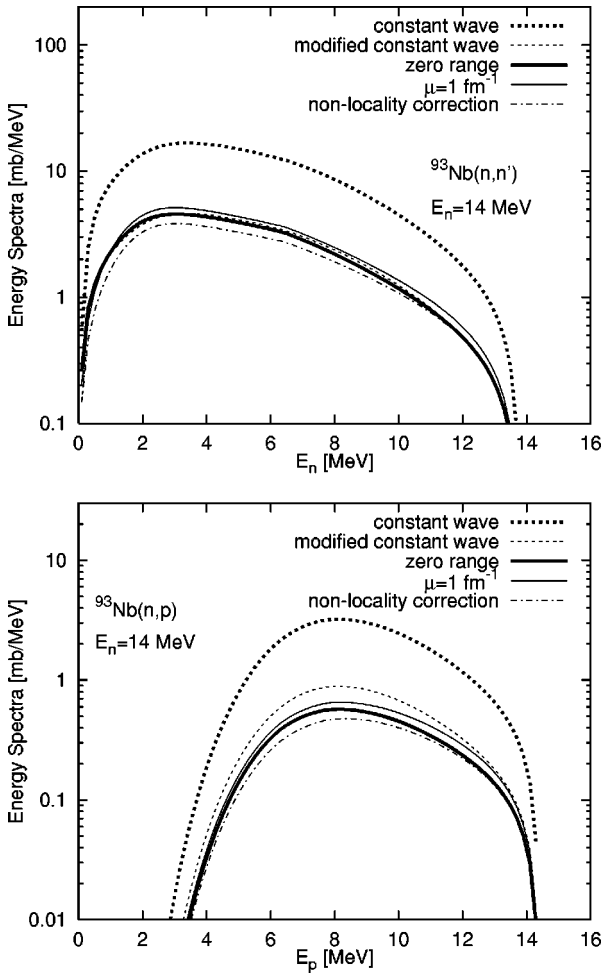

FIG. 7. Comparisons of the total MSC emission spectra of neutron-induced reactions on ^{93}Nb. The solid lines are the results of the microscopic calculation, and the dotted lines are calculated with the constant wave approximation.

The parameters used were the Walter and Guss' optical potential [15], the single-particle state density parameter $g=A/13$, the spin cutoff parameter of Gruppelaar [12], and no pairing energy. The nonlocality correction with $\beta=0.85$ was adopted for both MSC and MSD. The level density parameter $a=13.0$ MeV^{-1} [25] was adopted to calculate the Hauser-Feshbach particle emission spectra, and the Hauser-Feshbach component was renormalized so as to conserve the total reaction cross section. The direct reaction and the multiple particle emission such as an $(n,2n)$ reaction were not taken into account.

At first, we tried to fit the calculated cross sections to the

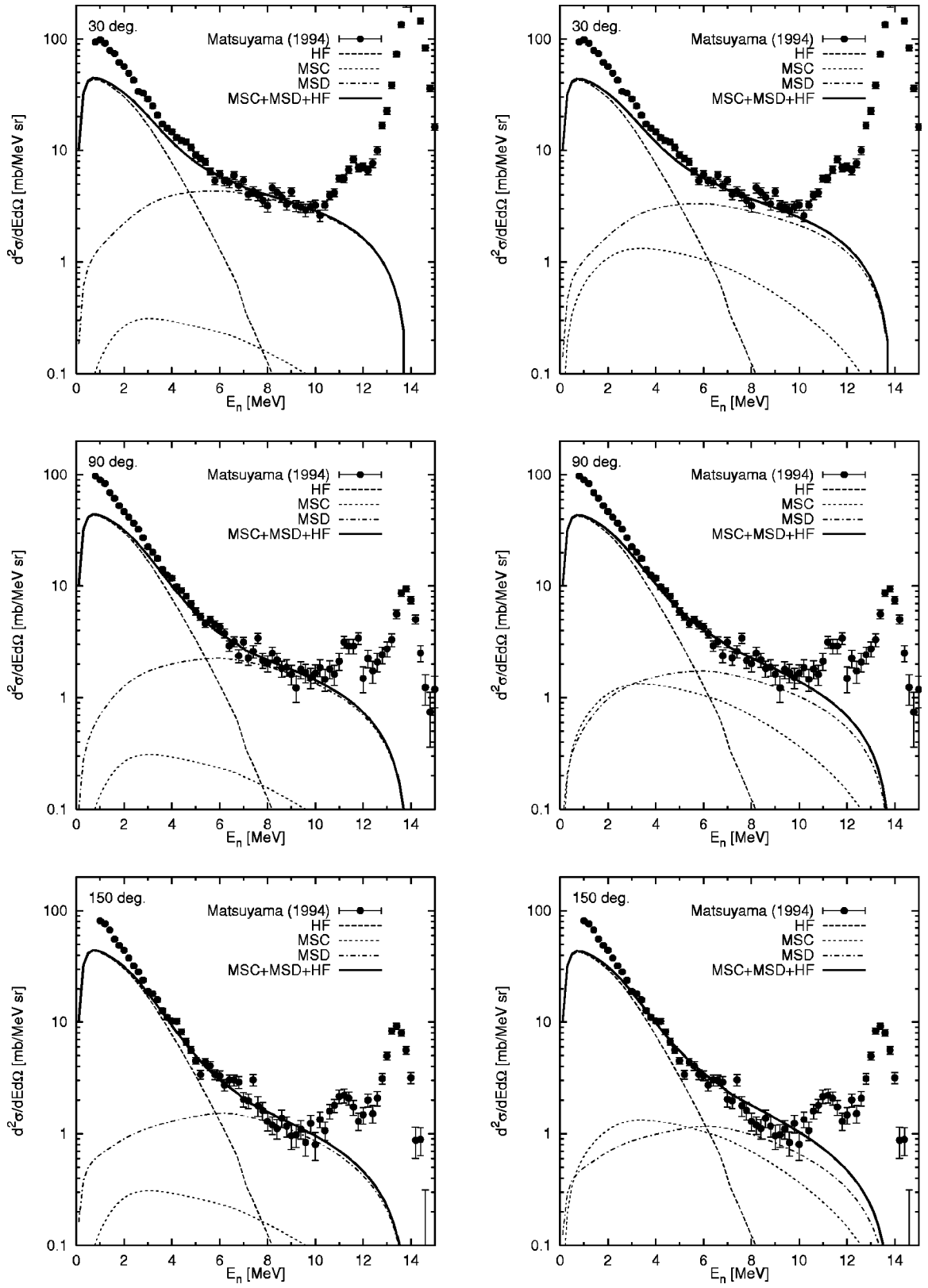

FIG. 8. Comparisons of the calculated double-differential cross sections of $n+{}^{93}\mathrm{Nb}$ reaction at $E_n=14.1$ MeV with the experimental data. The MSC process on the left side is calculated microscopically, and the right side shows the results with the constant wave approximation.

experimental double-differential cross section (DDX) data with the same V_0 value for both MSC and MSD. The obtained V_0 value at $E_n=14.1$ MeV was 45.0 MeV, and it was in accordance with the previous work [21]. However, the $2p$-$1h$ MSC doorway state formation cross section with this V_0 is 986 mb, which is twice as large as the cross section given by Eq. (17). If one equates the doorway state cross sections calculated from the phase-space model and the mi-

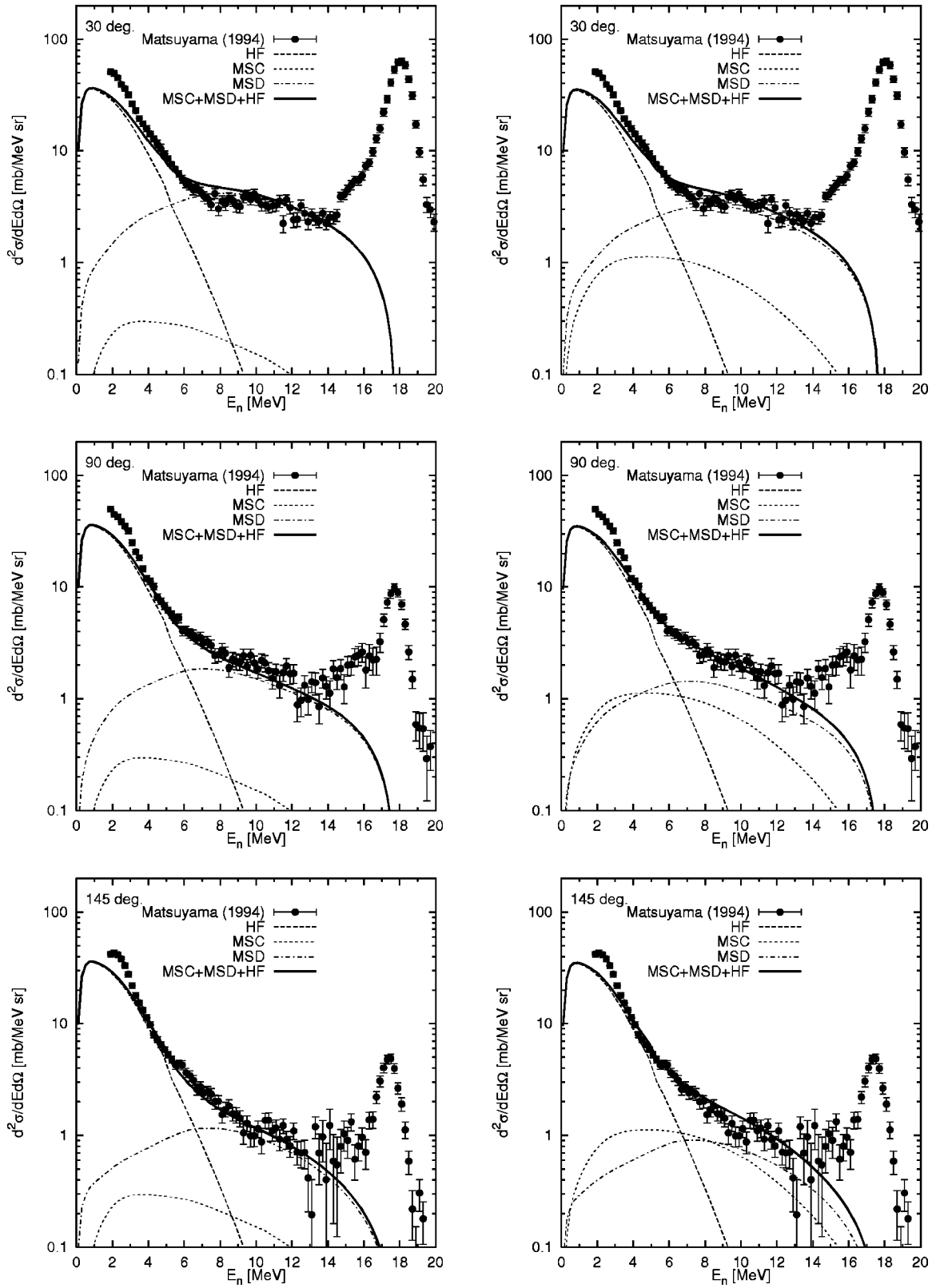

FIG. 9. Same as Fig. 8, but for $E_n = 18$ MeV.

croscopic model, the estimate of V_0 is 30.0 MeV; thus $V_0^{\mathrm{MSD}} = 1.5 V_0^{\mathrm{MSC}}$. The problem of the difference between the V_0 values for MSC and MSD has not yet been solved. The two-component theory of Koning and Chadwick [4] has an impact on the V_0 value for the one-step MSD cross section. Further work is needed to obtain the consistent V_0 value for both MSC and MSD. At this moment, we allow the V_0 values to be different for MSC and MSD.

Comparisons of the calculated DDX spectra with the experimental data at $E_n = 14.1$ MeV are shown in Fig. 8, on

the left side. The value of $V_0^{\mathrm{MSC}}=30.0$ MeV, which was derived from the phase-space model, was adopted for the calculation of the MSC spectra. This value was fixed, and V_0^{MSD} was adjusted to the experimental data. The obtained V_0^{MSD} is 47.3 MeV. The calculated DDX spectra are in good agreement with the experimental data from the forward (30°) to the backward angles (150°).

The calculations of the MSC and MSD spectra in Fig. 8 include the nonlocality correction. If this correction is excluded, $V_0^{\mathrm{MSC}}=23.2$ MeV and $V_0^{\mathrm{MSD}}=35.6$ MeV give almost the same fitting to the experimental data.

So far the constant wave approximation have been applied to analyze experimental DDX data. The right side in Fig. 8 shows the calculated DDX spectra with the constant wave approximation. The obtained V_0^{MSD} is 41.4 MeV, which is consistent with the published value, 42.8 ± 2.1 MeV of Watanabe *et al.* [21]. They employed the FKK-GNASH code [8], and fitted to the different experimental data set [26].

The MSC components calculated with the constant approximation are much larger than those calculated microscopically. The total MSC emission cross section with the constant wave approximation is 138 mb, while the microscopic calculation is 30.5 mb. The ratio of those cross sections is 0.22, which is consistent with the correction factor $3/2R=0.276$ proposed in Sec. III A. The increase in the MSC emission can be compensated for by the reduction of the MSD emission. Thus it is possible to obtain a good fit to the experimental DDX spectra even if the MSC cross section is four times larger. However, the difference appears at the backward angles. At 150°, the calculated spectrum exceeds the experimental data in the energy range of 7–10 MeV. This overestimation does not occur for the microscopic calculation.

Figure 9 shows the comparisons of the calculated DDX spectra with the experimental data at $E_n=18$ MeV. The drawings on the left side show the results of the microscopic calculation, and those on the right side are the case of the constant wave approximation. The V_0^{MSC} value of 29.3 MeV was obtained from the phase-space model. The obtained V_0^{MSD}'s are 39.7 MeV for the microscopic calculation, and 35.0 MeV for the constant wave approximation. The latter is consistent with the value of 36.0 ± 3.6 MeV in Ref. [21] within the uncertainty. The fitting to the DDX data at backward angles was difficult when the constant wave approximation was employed. This difficulty is due to the large MSC emission there. Since the microscopic calculation yields the smaller MSC emission, it results in a good fit to the experimental data at backward angles.

V. CONCLUSION

The microscopic calculations of the MSC process were compared with the simple MSC model which has been adopted in the data analysis with the FKK theory. Particle emission spectra with the microscopic model resulted in considerably smaller cross sections in comparison with the constant wave function approximation, although the shape of energy spectra is almost the same. If the cross sections with the constant wave function approximation are corrected by the factor of $3/2R$, where R is the nuclear radius, the difference between them becomes very small.

An energy dependence of the $2p$-$1h$ doorway state formation cross section calculated with the microscopic model was almost the same as that obtained with the phase-space model. A comparison of the microscopic calculation with the phase-space model calculation yielded a rough estimation of the residual interaction strength V_0. In the case of the zero-range interaction, V_0 was about 12.0 MeV for neutron-induced reactions on ^{93}Nb. The strength increased to 23.3 MeV if a Yukawa interaction with the range of 1 fm was assumed. When the nonlocality correction with $\beta=0.85$ was incorporated, the strength became 30.0 MeV.

The microscopically calculated MSC spectra were compared with the experimental data of double-differential cross sections at $E_n=14.1$ and 18.0 MeV. The one-step MSD and Hauser-Feshbach statistical emissions were added to the MSC spectra, and fitting of the calculated spectra to the experimental data yielded the strength of residual interaction V_0 for MSD. It was found that the obtained V_0 value for MSD differs from V_0 value of MSC. The microscopic MSC calculations gave smaller emission spectra than those with the constant wave approximation, and a fitting to the data at backward angles were improved.

ACKNOWLEDGMENTS

The author wishes to thank Y. Watanabe, M. Kawai, S. Yoshida, and H. Nakashima for valuable discussions.

[1] H. Feshbach, A. Kerman, and S. Koonin, Ann. Phys. (N.Y.) **125**, 429 (1980).
[2] T. Tamura, T. Udagawa, and H. Lenske, Phys. Rev. C **26**, 379 (1982).
[3] H. Nishioka, H. A. Weidenmüller, and S. Yoshida, Ann. Phys. (N.Y.) **183**, 166 (1988).
[4] A. J. Koning and M. B. Chadwick, Phys. Rev. C **56**, 970 (1997).
[5] R. Bonetti, L. Colli Milazzo, A. De Rosa, G. Inglima, E. Perillo, M. Sandoli, and F. Shahin, Phys. Rev. C **21**, 816 (1980).
[6] M. B. Chadwick, R. Bonetti, and P. E. Hodgson, J, Phys. G **15**, 237 (1989).
[7] R. Bonetti, L. Colli Milazzo, and M. Melanotte, Phys. Rev. C **27**, 1003 (1983).
[8] M. B. Chadwick and P. G. Young, Phys. Rev. C **47**, 2255 (1993).
[9] R. Bonetti, L. Colli Milazzo, and M. Melanotte, Lett. Nuovo Cimento **31**, 33 (1981).
[10] R. Bonetti and M. B. Chadwick, computer code GAMME (unpublished).
[11] R. Bonetti, M. B. Chadwick, P. E. Hodgson, B. V. Carlson, and M. S. Hussein, Phys. Rep. **202**, 171 (1991).
[12] H. Gruppelaar, ''IAEA Advisory Group Meeting on Basic and Applied Problems on Nuclear Level Densities,'' Brookhaven

National Laboratory report, 1983 (unpublished), p. 143.
[13] E. Gadioli and P. E. Hodgson *Pre-Equilibrium Nuclear Reactions* (Clarendon, Oxford, 1992).
[14] G. R. Satchler, Nucl. Phys. **55**, 1 (1964).
[15] R. L. Walter and P. P. Guss, Radiat. Eff. **95**, 73 (1986).
[16] P. A. Seeger and W. M. Howard, Nucl. Phys. **A238**, 491 (1975).
[17] E. V. Lee and J. J. Griffin, Phys. Rev. C **5**, 1713 (1972).
[18] R. Bonetti and L. Colombo, Phys. Rev. C **28**, 980 (1983).
[19] M. B. Johnson, L. W. Owen, and G. R. Satchler, Phys. Rev. **142**, 748 (1966).
[20] H. Kalka, Z. Phys. A **341**, 289 (1992).
[21] Y. Watanabe, A. Aoto, H. Kashimoto, S. Chiba, T. Fukahori, K. Hasegawa, M. Mizumoto, S. Meigo, M. Sugimoto, Y. Yamanouti, N. Koori, M. B. Chadwick, and P. E. Hodgson, Phys. Rev. C **51**, 1891 (1995).
[22] F. G. Perey and B. Buck, Nucl. Phys. **32**, 353 (1962).
[23] M. Baba, S. Matsuyama, T. Ito, T. Ohkubo, and N. Hirakawa, J. Nucl. Sci. Technol. **31**, 757 (1994).
[24] F. C. Williams, Nucl. Phys. **A166**, 231 (1971).
[25] N. Yamamuro, JAERI-M 90-006 (1990) (unpublished).
[26] A. Takahashi, M. Gotoh, Y. Sasaki, and H. Sugimoto, Osaka University, OKTAVIAN Report No. A-92-01 (1992) (unpublished).